Pyruvate Kinase M1 Suppresses Development and Progression of Prostate Adenocarcinoma

Shawn M. Davidson[1,2,3], Daniel R. Schmidt[1,3,4], Julia E. Heyman[1], James P. O'Brien[1], Amy C. Liu[1], William J. Israelsen[1,2], Talya L. Dayton[1,2], Raghav Sehgal[5], Roderick T. Bronson[1], Elizaveta Freinkman[6], Howard H. Mak[1], Giuseppe Nicolò Fanelli[7,8], Scott Malstrom[1], Gary Bellinger[1,4], Arkaitz Carracedo[4], Pier Paolo Pandolfi[4], Kevin D. Courtney[9], Abhishek Jha[5], Ronald A. DePinho[9], James W. Horner[9], Craig J. Thomas[10], Lewis C. Cantley[4,7], Massimo Loda[7,9], and Matthew G. Vander Heiden[1,2,3,9]

ABSTRACT

Altered metabolism helps sustain cancer cell proliferation and survival. Most cancers, including prostate cancers, express the M2 splice isoform of pyruvate kinase (PKM2), which can support anabolic metabolism to support cell proliferation. However, *Pkm2* expression is dispensable for the formation and growth of many cancers *in vivo*. Expression of pyruvate kinase isoform M1 (*Pkm1*) is restricted to relatively few tissues and has been reported to promote growth of select tumors, but the role of PKM1 in cancer has been less studied than PKM2. To test how differential expression of pyruvate kinase isoforms affects cancer initiation and progression, we generated mice harboring a conditional allele of *Pkm1* and crossed these mice, or those with a *Pkm2* conditional allele, with a *Pten* loss-driven prostate cancer model. *Pkm1* loss led to increased PKM2 expression and accelerated prostate cancer development, whereas *Pkm2* deletion led to increased PKM1 expression and suppressed tumor progression. Metabolic profiling revealed altered nucleotide levels in tumors with high PKM1 expression, and failure of these tumors to progress was associated with DNA replication stress and senescence. Consistent with these data, a small molecule pyruvate kinase activator that mimics a high activity PKM1-like state suppressed progression of established prostate tumors. Analysis of human specimens showed PKM2 expression is retained in most human prostate cancers. Overall, this study uncovers a role for pyruvate kinase isoforms in prostate cancer initiation and progression, and argues that pharmacologic pyruvate kinase activation may be beneficial for treating prostate cancer.

Significance: Differential expression of PKM1 and PKM2 impacts prostate tumorigenesis and suggests a potential therapeutic vulnerability in prostate cancer.

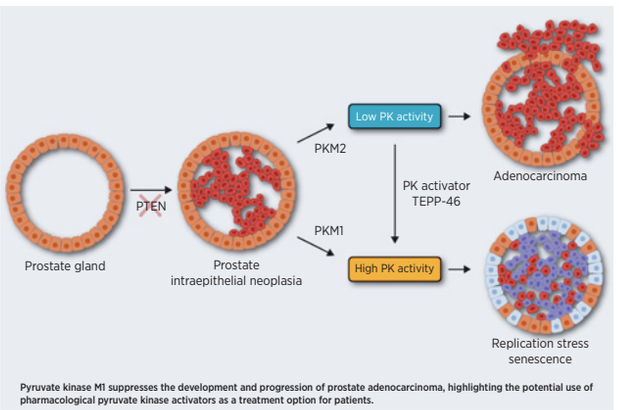

Pyruvate kinase M1 suppresses the development and progression of prostate adenocarcinoma, highlighting the potential use of pharmacological pyruvate kinase activators as a treatment option for patients.

Introduction

Prostate cancer is the second leading cancer-related cause of death in men and given time most men will develop prostate cancer (1). Loss of the tumor suppressive lipid phosphatase PTEN is associated with abnormal prostate growth in prostate cancer, with many prostate cancers exhibiting decreased *PTEN* expression due to mutation or epigenetic silencing (2–4). Loss of PTEN activity results in phosphatidylinositol (3, 4, 5)-triphosphate accumulation and activation of AKT signaling to drive uncontrolled proliferation and survival (5, 6). How these signaling events promote prostate cancer have been extensively studied (7), as have the ways in which growth factor signaling

[1]Koch Institute for Integrative Cancer Research, Massachusetts Institute of Technology, Cambridge, Massachusetts. [2]Department of Biology, Massachusetts Institute of Technology, Cambridge, Massachusetts. [3]Broad Institute of MIT and Harvard University, Cambridge, Massachusetts. [4]Beth Israel Deaconess Medical Center, Boston, Massachusetts. [5]Elucidata, Cambridge, Massachusetts. [6]Whitehead Institute, Cambridge, Massachusetts. [7]Weill Cornell Medical College, New York, New York. [8]Division of Pathology, Department of Translational Research and New Technologies in Medicine and Surgery, University of Pisa, Pisa, Italy. [9]Dana-Farber Cancer Institute, Boston, Massachusetts. [10]National Center for Advancing Translational Sciences, NIH, Bethesda, Maryland.

Note: Supplementary data for this article are available at Cancer Research Online (http://cancerres.aacrjournals.org/).

D.R. Schmidt, J.E. Heyman, J.P. O'Brien, and A.C. Liu contributed equally to this article.

Current address for S.M. Davidson: Lewis Sigler Institute, Princeton University, Princeton, New Jersey; current address for W.J. Israelsen: University of Texas Southwestern Medical Center, Dallas, Texas; current address for A. Carracedo: Center for Cooperative Research in Biosciences (CIC bioGUNE), Derio, Spain and Ikerbasque, Basque Foundation for Science, Bilbao, Spain; current address for Pier Paolo Pandolfi: Renown Cancer Institute, Nevada System of Higher Education, Reno, Nevada; and current address for R.A. DePinho: University of Texas MD Anderson Cancer Center, Houston, Texas.

Corresponding Authors: Matthew G. Vander Heiden, Koch Institute/Biology, Massachusetts Institute of Technology, Cambridge, MA 02139. E-mail: mvh@mit.edu; and Shawn M. Davidson, shawnd@princeton.edu

Cancer Res 2022;82:2403–16

doi: 10.1158/0008-5472.CAN-21-2352

pathways can affect cell metabolism (8, 9). However, whether changes in metabolic enzyme expression affect prostate tumor initiation and progression is less well defined.

Changes in metabolism are necessary to sustain cancer cell proliferation (9, 10). Many cancer cells exhibit increased glucose uptake (10, 11). Increased tumor glucose consumption relative to normal tissues is exploited clinically to stage cancers through utilization of ^{18}FDG-PET imaging (12); however, most prostate cancers grow at a slower rate than highly ^{18}FDG-avid malignancies and ^{18}FDG-PET is not often used in the clinical management of patients with prostate cancer, leading to the notion that these cancers rely less on glucose metabolism (13). Nevertheless, prostate cancer cells metabolize glucose in culture (14, 15), and ^{18}FDG-PET avidity is observed in prostate cancer, including aggressive tumors (16, 17). Whether changes in glucose metabolism influence prostate cancer initiation and progression has not been extensively studied.

Induction of cellular senescence can suppress cancer development (18–20). Overcoming cellular senescence is thought to be particularly important in the pathogenesis of some prostate cancers, as *Pten* loss results in a p53-dependent senescence response by prostate epithelial cells in preclinical models (21), and can suppress tumor formation (18, 20). Changes in metabolism to increase glucose oxidation can promote senescence in some tissues (22) and senescent lesions can be hypermetabolic (23). Cellular senescence is also associated with decreased anaplerotic flux into the tricarboxylic acid cycle (24), and nucleotide deficiency can promote this phenotype by promoting DNA replication stress (25). Of note, loss of *Pten* in prostate epithelial cells can cause DNA replication stress, induce a DNA damage response, and contribute to senescence (26). Taken together, these studies suggest that changes in metabolism that affect nucleotides and DNA replication can contribute to the induction or maintenance of a quiescent or senescent state; however, the relationship between metabolism and tumor suppression due to cellular senescence is controversial (23, 27, 28), and whether changes in glucose metabolism influence senescence as a tumor suppressive mechanism in prostate cancer is not known.

Regulation of pyruvate kinase activity can influence the extent of glucose oxidation and nucleotide synthesis (29–31). Most human and murine tissues express an isoform of pyruvate kinase that is encoded by the *PKM* gene (32, 33). This gene produces an RNA product that is alternatively spliced to generate mRNAs encoding two different isoforms of the enzyme: PKM1 and PKM2 (34). The mRNA encoding PKM1 and PKM2 differ only in inclusion of either exon 9 for the PKM1 message or exon 10 for the PKM2 message. PKM1 is a constitutively active enzyme that promotes oxidative glucose metabolism (29, 32). PKM2 is allosterically regulated, and decreased pyruvate kinase activity associated with this isoform can promote anabolic metabolism including nucleotide synthesis (32, 35). Genetic deletion of the *Pkm2*-specific exon in proliferating primary mouse embryonic fibroblasts that normally express PKM2 results in PKM1 expression and an irreversible proliferation arrest (31). Moreover, deleting only one *Pkm2* allele also results in PKM1 expression that leads to proliferation arrest despite continued expression of PKM2 at wild-type levels, indicating that expression of PKM1 rather than loss of PKM2 is responsible for the phenotype (31). Proliferation arrest caused by PKM1 expression can be prevented by addition of exogenous nucleotide bases (31), suggesting that high pyruvate kinase activity associated with PKM1 expression can limit nucleotide synthesis, but whether this results in tumor suppression is not known.

Although most tissues in mice express either the *Pkm1* or *Pkm2* isoform of pyruvate kinase (33), cancer cells preferentially express *Pkm2* (32, 36). This is thought to be advantageous to cancer cells because PKM2 expression allows cells to adapt pyruvate kinase activity to different cell conditions (35, 37); however, why PKM2 is selected for in most cancers is controversial (33, 38). Pyruvate kinase is active as a homotetramer (30, 39, 40). Allosteric regulators that decrease PKM2 activity function by destabilizing the active tetramer. In contrast, PKM1 is constitutively active because residues encoded by the isoform-specific exon promote stable tetramer formation. Small molecule pyruvate kinase activators have been identified that stabilize the PKM2 tetramer to promote an enzyme state similar to PKM1 (30, 41–43). One such PKM2 activator, TEPP-46, is bioavailable when dosed orally in mice and can inhibit xenograft growth, phenocopying the effects of PKM1 expression (30). However, *Pkm2* expression is not required for tumor growth in several mouse cancer models (33, 44–50), suggesting that loss of *Pkm2* expression might limit the ability of pyruvate kinase activators to be effective cancer drugs.

Whether high pyruvate kinase activity due to PKM1 expression is a barrier to cancer initiation is not known. PKM1 expression is reported to provide a metabolic advantage to tumors in some contexts (38), and suppress tumor growth in others (29, 30, 45). Because PKM1 is constitutively active, understanding where PKM1 expression suppresses tumor growth could inform which tumor types might be sensitive to pyruvate kinase activating drugs. To study how PKM1 expression affects tumor formation, we generated mice harboring a conditional allele for the unique exon included in *Pkm1*. We crossed animals harboring this *Pkm1*-conditional allele, as well as mice harboring a *Pkm2*-conditional allele (45), to a *Pten* loss-driven mouse prostate cancer model (21, 51). We found that PKM isoform expression profoundly impacts prostate tumor initiation and progression. Deletion of both *Pkm1* and *Pten* in the prostate results in the formation of aggressive prostate tumors that limit animal survival. In contrast, deletion of *Pkm2* and *Pten* in the prostate results in high *Pkm1* expression and suppresses tumor formation. Importantly, small molecule PKM2 activators can also suppress prostate tumor growth, and many human prostate cancers retain PKM2 expression, arguing that forcing pyruvate kinase into a high activity state might have a role in managing prostate cancer in patients.

Materials and Methods

Generation and breeding of Pkm1 conditional mice and mouse strains

The conditional allele for *Pkm1* was generated using standard protocols to introduce loxP sites in the intronic region flanking exon 9 of the *Pkm1* gene in a manner analogous to how the *Pkm2* allele was generated (see ref. 45). For all experiments, the *PbCre4* (MGI:2385927) allele was maintained in males due to previously observed germline recombination and mosaic expression of floxed alleles when the *PbCre4* allele is transmitted through females (52). Males harboring *PbCre4, Pten* (MGI:2679886), *Pkm1*, or *Pkm2* (MGI: 5547750) floxed alleles were crossed to females harboring *Pten*, *Pkm1*, or *Pkm2* floxed alleles to generate prostate restricted deletion of these genes and splice products. All animals were maintained on a mixed background and littermates were used for direct comparisons.

[^{18}F]-2-deoxyglucose PET

Animals were fasted overnight before administration of 100 μCi of FDG ^{18}F through a tail-vein catheter. Animals were kept warm using a heated water pad and placed under 2% anesthesia during the 1 hour uptake time to lower background signal. Because of the small size of the prostate and its proximity to the bladder in 7- to 11-week-old control

and *Pten*$^{pc-/-}$ animals, tissue was harvested after FDG administration and gamma counts used to assess FDG uptake in prostate and gastrocnemius muscle tissue. For studies involving 6-month-old mice, animals were imaged for 10 minutes by PET and 1 minute by CT using 720 projections at 50 kV and 200 μA using Sofie G8 PET/CT. Images were CT attenuation corrected and MLEM3D reconstructed. All images were decay corrected to the time of injection. The average signal intensity for three regions of each prostate was normalized to the average signal intensity for three regions in the heart of each animal.

Southern blot analysis

Asp718 (Roche)-digested genomic DNA was analyzed by Southern blot using standard protocols and probe binding was visualized by autoradiography using an analogous strategy to what was described previously for the *Pkm2* allele (45). Asp718 has the same restriction site specificity as Kpn1.

PCR genotyping

PCR genotyping for *Pkm1* conditional mice was developed to detect and amplify the targeted *Pkm* genetic locus and performed using forward (5′-CACGCAACCATTCCAGGAGCATAT-3′) and reverse (5′-TGGTGACCTTGGCTGTCTTCCTGA-3′) primers. To genotype *PbCre4*, forward (5′-CTGAAGAATGGGACAGGCATTG-3′) and reverse (5′-CATCACTCGTTGCATCGACC-3′) primers were used as suggested by the NCI mouse repository. Genotyping of the *Pten and Pkm2* alleles used in this study was performed as described previously (45, 53).

Western blot analysis and IHC analysis of mouse tumors

Western blots were performed using primary antibodies against PKM1 (Sigma-Aldrich, catalog no. SAB4200094, RRID:AB_10624711), PKM2 (Cell Signaling Technology, catalog no. 4053, RRID:AB_1904096), PKM (Cell Signaling Technology, catalog no. 3190, RRID:AB_2163695; Abcam, catalog no. ab6191, RRID:AB_2163678), and vinculin (Sigma-Aldrich, catalog no. V4505, RRID:AB_477617). For IHC, the following primary antibodies were used: 1:600 PKM1 (Cell Signaling Technology, catalog no. 7067, RRID:AB_2715534), 1:1,200 PKM2 (Cell Signaling Technology, catalog no. 4053, RRID:AB_1904096), 1:100 phospho-CHK1 (ser317) (MyBioSource, catalog no. MBS9600779), 1:300 vimentin (Abcam, catalog no. ab24525, RRID:AB_778824), 1:200 pancytokeratin (Abcam, catalog no. ab9377, RRID:AB_307222); 1:200 synaptophysin (Thermo Fisher Scientific, catalog no. PA5–16417, RRID:AB_10989504), 1:16,000 PCNA (Cell Signaling Technology, catalog no. 2586, RRID:AB_2160343), 1:100 Ki-67 (BD Pharmingen, catalog no. 556003), 1:100 AR (Santa Cruz, catalog no. sc-816-G). IHC analysis of PKM1 and PKM2 in mouse tissue sections was performed as follows: 5-μmol/L-thick formalin-fixed paraffin-embedded (FFPE) tissue sections were deparaffinized and immediately underwent heat-mediated antigen retrieval in a pressure cooker at 125°C for 5 minutes in Citra pH 6.0 solution (Biogenex, catalog no. HK086). Endogenous peroxidase activity was quenched with BLOXALL (Vector Labs, catalog no. SP-6000) for 20 minutes. Sections were then blocked with Protein Block (Dako, catalog no. X0909) for 30 minutes, incubated overnight with primary antibody at 4°C, incubated with SignalStain Boost (Cell Signaling, catalog no. 8114) for 30 minutes, incubated with SignalStain DAB substrate (Cell Signaling, catalog no. 8059) for 2 minutes (PKM2) or 5 minutes (PKM1) at room temperature, and counterstained with hematoxylin. IHC analysis of pChk1 was performed as follows: 5-μmol/L-thick FFPE tissue sections were deparaffinized and immediately underwent heat-mediated antigen retrieval in a pressure cooker at 125°C for 5 minutes in Citra pH 6.0 solution (Biogenex, catalog no. HK086), Endogenous peroxidase activity was quenched with BLOXALL (Vector Labs, catalog no. SP-6000) for 20 minutes. Sections were then blocked for 30 minutes with 3% normal goat serum, incubated overnight with primary antibody at 4°C, incubated with avidin/biotin/HRP reagents per manufacturer recommended protocol (Vector Labs ABC-HRP Kit, catalog no. PK-4001), incubated with DAB substrate (Vector Labs, catalog no. SK-4100) for 5 minutes at room temperature, and counterstained with hematoxylin. For all other primary antibodies, incubation was at room temperature for 1 hour. For all other primary antibodies except vimentin, IHC analysis was performed as described above for pCHK1. Vimentin was detected with an AP-conjugated goat-anti-chicken (Thermo Fisher Scientific, catalog no. PA1–28799, RRID:AB_10984880) and stained with Vulcan Fast Red Kit 2 (Biocare, catalog no. FR805). Staining intensity for PKM1, PKM2, and pChk1 in mouse prostate tumors was scored using a 4-category system (negative, low, intermediate, high). Three high power fields per tumor were evaluated and each assigned to a staining intensity category based on the most prevalent staining intensity patterns of tumor cells within that field. The tumor was assigned the median category. Percent Ki-67 positive cells in anterior prostate tumors of Pten$^{pc-/-}$ mice treated with TEPP-46 for 4 weeks ($n = 2$) and age matched controls ($n = 4$) was quantitated using an automated algorithm in QuPath (Version: 0.3.0; ref. 54). Ten high-power fields were selected per tumor. Within each high-power field, areas containing tumor cells were manually selected to generate a region of interest (ROI). Total number of tumor cells and Ki-67 positive cells per ROI were quantitated using the analyze → cell detection → positive cell detection function with the following parameters: setup parameters (hematoxylin OD, pixel size = 0.5 μmol/L), nucleus parameters (background radius = 8 μmol/L, median filter radius = 0 μmol/L, sigma = 1.5 μmol/L, min area = 10 μm^2, max area = 400 μm^2), intensity parameters (threshold = 0.1, max background intensity = 2, split by shape selected), cell parameters (cell expansion = 5 μmol/L, include cell nucleus selected), general parameters (smooth boundaries selected, make measurements selected), intensity threshold parameters (nucleus DAB OD mean, single threshold). Percentage of Ki-67-positive cells equals Ki-67-positive cells divided by total number of tumor cells. All Ki-67 quantification was done by scoring sections in a blinded fashion.

MRI

For longitudinal measurements of tumor growth, WT, *Pten*$^{pc-/-}$, *Pten;Pkm1*$^{pc-/-}$, or *Pten;Pkm2*$^{pc-/-}$ littermates were randomized into cohorts and prostate tissue size assessed biweekly using a Varian 7T MRI imaging system. Image sequences were acquired using the proton imaging FSEMS sequence (fast spin echo multiple slice) with TR: 4,000 milliseconds; TE: 12 milliseconds in the axial orientation. Additional settings were as follows: 256 × 256 data matrix; 45 × 45 mm region; 1-mm-thick slice; for 20 slices. OsiriX-Viewer was used for image analysis. MRI assessment of abnormal prostate growth was noted when the prostate tissue volume increased over at least two consecutive timepoints.

β-Galactosidase senescence staining of tissues

β-Galactosidase staining was conducted as reported previously (55). In brief, fresh frozen sections were cut to 8 μm thickness and briefly fixed in paraformaldehyde. A solution containing 1 mg of 5-bromo-4-chloro-3-indoyl β-D-galactoside (X-gal) per mL (diluted from a stock of 20 mg of dimethylformamide per mL) with 40 mmol/L citric acid/sodium phosphate pH 5.5, 5 mmol/L potassium ferricyanide in

150 mmol/L $NaCl_2$, and 2 mmol/L $MgCl_2$ was applied to the tissue. Sections were incubated in a CO_2 free incubator at 37°C for 12 to 16 hours and then visualized by conventional light microscopy.

Metabolite measurement and analysis

For metabolite extraction, 10 to 40 mg of anterior prostate tissue was weighed and homogenized cryogenically (Retsch Cryomill) prior to extraction in chloroform:methanol:water (4:6:3). Samples were centrifuged to separate aqueous and organic layers, and polar metabolites were dried under nitrogen gas for subsequent analysis by mass spectrometry. For LC/MS, dried metabolites were resuspended in water based on tissue weight, and valine-D8 was used as an injection control (56). LC/MS analyses were conducted on a QExactive benchtop orbitrap mass spectrometer equipped with an Ion Max source and a HESI II probe, which was coupled to a Dionex UltiMate 3000 UPLC system (Thermo Fisher Scientific). External mass calibration was performed using the standard calibration mixture every 7 days. Sample was injected onto a ZIC-pHILIC 2.1 × 150 mm (5 μm particle size) column (EMD Millipore). Buffer A was 20 mmol/L ammonium carbonate, 0.1% ammonium hydroxide; buffer B was acetonitrile. The chromatographic gradient was run at a flow rate of 0.150 mL/min as follows: 0 to 20 minutes: linear gradient from 80% to 20% B; 20 to 20.5 minutes: linear gradient from 20% to 80% B; 20.5 to 28 minutes: hold at 80% B. The mass spectrometer was operated in full-scan, polarity switching mode with the spray voltage set to 3.0 kV, the heated capillary held at 275°C, and the HESI probe held at 350°C. The sheath gas flow was set to 40 units, the auxiliary gas flow was set to 15 units, and the sweep gas flow was set to 1 unit. The MS data acquisition was performed in a range of 70 to 1,000 *m*/*z*, with the resolution set at 70,000, the AGC target at 106, and the maximum injection time at 80 milliseconds. Relative quantitation of polar metabolites was performed with XCalibur QuanBrowser 2.2 (Thermo Fisher Scientific) using a 5 ppm mass tolerance and referencing an in-house library of chemical standards.

PCA analysis was performed using MetaboAnalyst 4.0 (McGill University). The input dataset included 111 metabolites that were detectable in primary prostate tumors of all three genotypes and wild-type prostate (four groups total). The dataset was filtered for metabolites with near-constant values by IQR. Missing values (0.7%) were replaced with a value equal to half of the minimum value detected (assumed to be the detection limit) for a given metabolite. Peak areas were log transformed and centered at the mean.

TEPP-46 treatment of *Pten*$^{pc-/-}$ mice

Six-month-old *Pten*$^{pc-/-}$ animals were serially imaged using MRI until tumors were estimated to be >2 mm^3, and then randomized to receive either PKM2 activator (TEPP-46) or a vehicle control delivered twice daily via oral gavage at a final dose of 50 mg/kg in a volume less than 250 μL for 4 weeks. The ages of mice treated varied from 8 to 18 months with cohorts selected on the basis of tumor size. TEPP-46 was formulated in 0.5% carboxymethyl cellulose with 0.1% v/v Tween 80 as reported previously (30).

IHC analysis of human prostate cancer

PKM1 and *PKM2* expression was determined by IHC in clinically annotated human prostate cancer tissue sections collected at Dana-Farber Cancer Institute during routine clinical care. Collection of tissue was approved by the Institutional Review Board of the Dana Farber Cancer Institute (Protocol 01–045) and Partners Healthcare (IRB 2006P000139). Briefly, FFPE prostate tissue from 345 patients (including three tumor cores and two matched normal cores per patient) were arrayed on seven panels. Tissue microarray (TMA) hematoxylin and eosin sections were reviewed by a board-certified genitourinary pathologist (ML) to confirm presence of tumor and normal prostate. Corresponding unstained TMA sections were stained with antibodies that detect either PKM1- or PKM2-specific epitopes as described above. In total, 304 patients for which adequate tumor or normal tissue was present were included in the final analysis. Each core was scored for PKM1 and PKM2 and assigned a categorical variable (negative, low, intermediate, or high) based on the intensity of staining. Each individual patient was assigned the median category of the three tumor cores (expression in tumor) and higher category of the two normal cores (expression in normal prostate).

Statistical analysis

Log-rank tests were performed to determine significance in survival or tumor incidence (SPSS Statistics). Two-tailed paired and unpaired Student *t* test were performed for all other experiments unless otherwise specified (GraphPad PRISM 7). Results for independent experiments are presented as mean ±SEM; results for technical replicates are presented as mean ±SD.

Declarations

All animal experiments were approved by the MIT Committee on Animal Care. All tissue analyzed from patients with prostate cancer was obtained via protocols approved by the Institutional Review Board of the Dana Farber Cancer Institute (Protocol 01–045) and Partners Healthcare (IRB 2006P000139), with written informed consent obtained from all patients, and the tissue collected in accordance with ethical guidelines.

Data availability

All data are included in the supplemental materials, or are available from the corresponding author upon reasonable request.

Results

PTEN deletion increases glucose uptake prior to formation of invasive prostate cancer

PTEN loss is sufficient to promote glucose uptake (57) even though silencing of *Pten* alone is not sufficient to transform prostate epithelial cells (58). PTEN is frequently lost in human prostate cancer (4), so to determine whether increased glucose uptake is an early consequence of *Pten* loss in the prostate, mice homozygous for a conditional *Pten* allele (*Pten*^{fl}) were crossed to mice with a *PbCre4* allele that drives prostate-specific Cre-recombinase expression, enabling the generation of animals with prostate-restricted *Pten* deletion (*Pten*$^{pc-/-}$; refs. 21, 51, 59). These mice develop prostatic intraepithelial neoplasia (PIN) at approximately 3 months of age, which progresses to invasive cancer as the mice age. To assess the effect of *Pten* loss on glucose uptake prior to the development of invasive cancers, we measured ^{18}FDG uptake in the prostate and muscle of *Pten*$^{pc-/-}$ mice at 7 to 11 weeks of age. Glucose uptake was elevated in the prostate but not the muscle of *Pten*$^{pc-/-}$ mice (**Fig. 1A**), even though this time point is prior to the onset of invasive cancer (21). These findings suggest that *Pten* loss is sufficient to increase glucose uptake in prostate tissue, and that increased glucose uptake can occur prior the development of histologically apparent neoplasia.

A shift in pyruvate kinase isoform expression accompanies prostate cancer initiation

Because *Pkm1* expression is sufficient to suppress proliferation in some cells despite high glucose uptake (31), we questioned whether

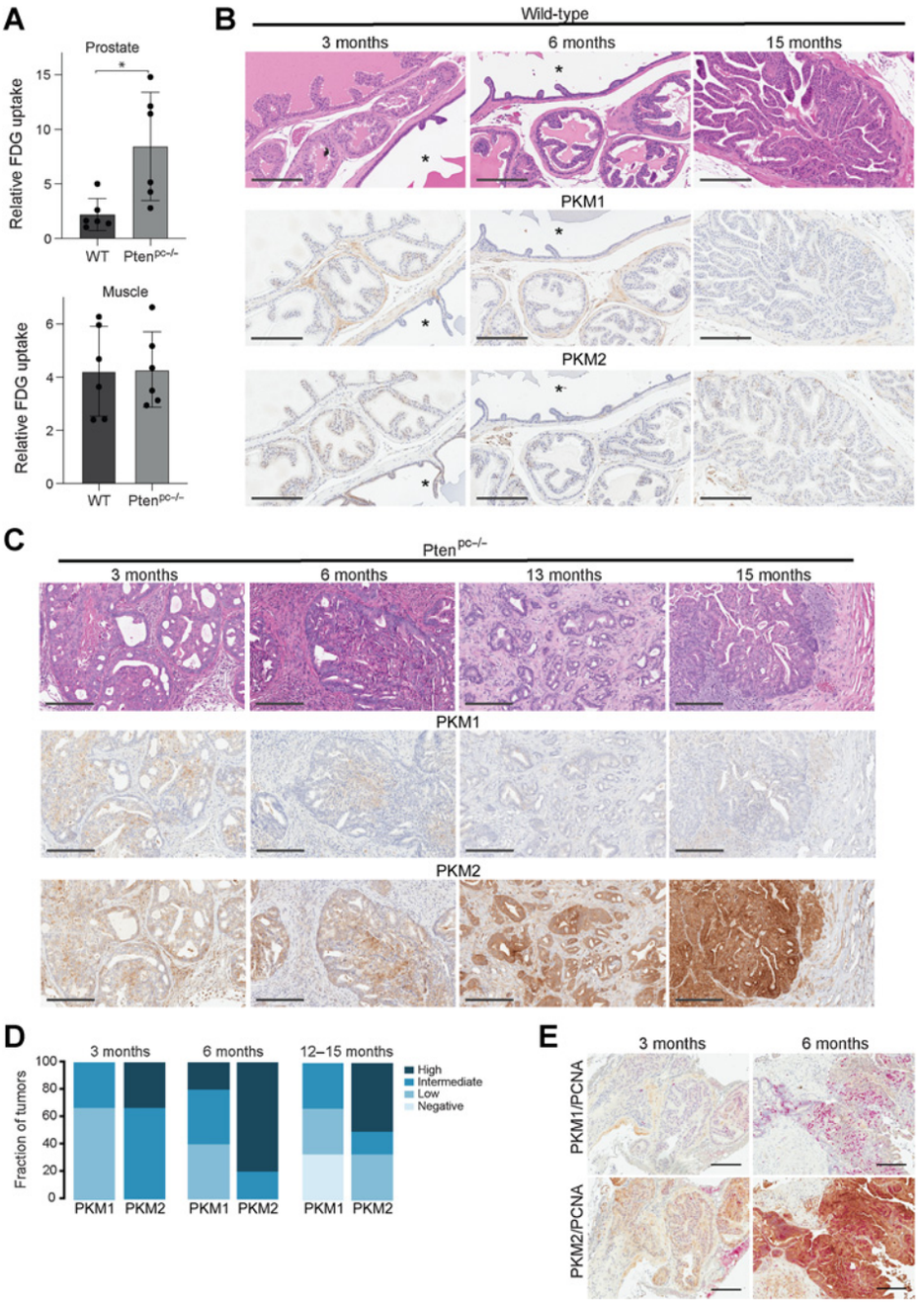

Figure 1.

Increased glucose uptake and a change in PKM isoform expression accompanies *Pten* loss in mouse prostate tissue. **A,** Relative FDG uptake into the anterior prostate and gastrocnemius muscle of 7- to 11-week-old WT mice and mice with prostate-specific *Pten* deletion ($Pten^{pc-/-}$). Mean ± SD is shown ($n = 6$). The difference in FDG uptake between genotypes is significant in prostate (*, $P < 0.05$ by Student t test), but not in muscle. **B,** Representative hematoxylin and eosin and IHC assessment of PKM1 and PKM2 expression in anterior prostate tissue harvested from WT mice of the indicated age. *, adjacent seminal vesicle tissue. Scale bar, 200 μm. **C,** Representative hematoxylin and eosin and IHC assessment of PKM1 and PKM2 expression in prostate tissue harvested from $Pten^{pc-/-}$ mice of the indicated age. Scale bar, 200 μm. **D,** Quantitation of PKM1 and PKM2 expression in prostate tissue harvested from $Pten^{pc-/-}$ mice of the indicated age as determined by IHC. Tissue from 3 to 6 mice per age group was quantified. **E,** Representative IHC staining of PKM1 or PKM2 (brown) and PCNA (pink) in tumors from $Pten^{pc-/-}$ mice of the indicated age. Scale bar, 200 μm.

changes in pyruvate kinase isoform expression might be associated with cancer formation in the prostate. The mouse prostate has three anatomically distinct lobes (60). Tumor formation in $Pten^{pc-/-}$ mice is most prominent in the anterior prostate (AP), and growth of anterior prostate tumors are the major cause of mortality in this cancer model (21, 61), therefore we focused on histopathologic characterization of tumors arising in this lobe. PKM isoform-specific antibodies were used to evaluate PKM isoform expression by IHC. Non-prostate tissues with known pyruvate kinase isoform expression were stained to confirm the specificity of antibody staining by IHC, and in young wild-type mice, PKM2 expression was found to be highest in epithelial cells throughout the prostate and seminal vesicles, whereas PKM1 expression was found to be highest in the stromal compartment, with weaker expression observed in epithelial cells (**Fig. 1B**; Supplementary Figs. S1A and S1B). Prostate intraepithelial neoplasia (PIN) lesions in 3-month-old $Pten^{pc-/-}$ mice were characterized by upregulation of PKM1 and PKM2 expression compared with normal prostate epithelium, and tumor associated stroma also showed increased PKM2 expression (**Fig. 1B** and **C**). Tumor progression from PIN to invasive disease in older mice was associated with increased expression of PKM2 and decreased expression of PKM1, and with androgen receptor expression (**Fig. 1C** and **D**; Supplementary Figs. S1C and S1D). Furthermore, we observed increased PKM2 and decreased PKM1 expression in prostate tumor regions with increased proliferation as

assessed by PCNA staining (**Fig. 1E**). These data suggest that in *Pten*-driven prostate cancer, increased PKM2 expression and loss of *Pkm1* expression is correlated with increased cell proliferation and tumor progression.

Generation of a conditional allele to prevent Pkm1 expression

To generate a conditional allele that eliminates *Pkm1* isoform expression in mouse tissues, we introduced loxP sites that flank the PKM1-isoform-specific exon 9 into the *Pkm* genomic locus of mouse embryonic stem (ES) cells using homologous recombination (**Fig. 2A**). Proper targeting of ES cells was confirmed by Southern blot analysis (Supplementary Fig. S2A). Targeted ES cells were used to generate chimeric mice, which were subsequently bred to achieve germline transmission of the conditional allele and then crossed to FLP recombinase transgenic mice to delete the Neo^r gene. Expected targeting of the *Pkm* genomic locus was confirmed in the animals by Southern blot analysis (**Fig. 2B**) and by a PCR-based approach developed for genotyping (Supplementary Fig. S2B). Intercrossing *Pkm1* conditional mice yielded progeny born in the expected Mendelian ratios that display no overt phenotypes.

To determine the effect of *Pkm1* deletion in the prostate, we crossed *Pkm1* conditional mice to animals with a *PbCre4* allele to achieve animals homozygous for the *Pkm1*^{fl} allele (*Pkm1*$^{fl/fl}$ *PbCre4*, hereafter *Pkm1*$^{pc-/-}$). Examination of *Pkm1* expression in the AP from these animals showed the expected decrease in *Pkm1* mRNA transcript levels (**Fig. 2C**), and the absence of PKM1 protein expression by Western blot analysis in all prostate lobes, whereas PKM1 protein

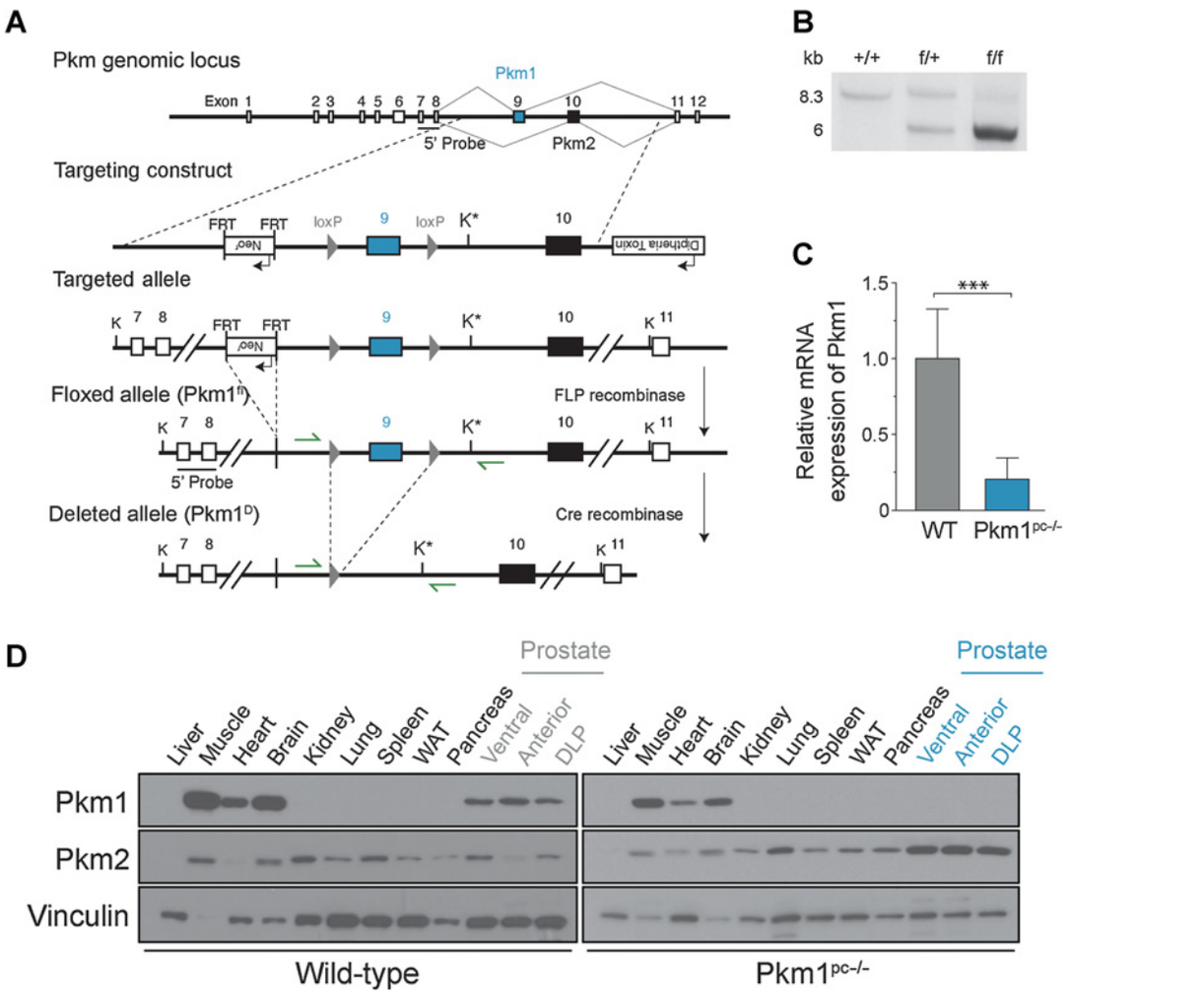

Figure 2.

Generation and validation of *Pkm1* conditional mice. **A,** A schematic showing the mouse *Pkm* locus, construct targeting *Pkm1*-specific exon 9, and the resulting targeted, floxed, and deleted *Pkm1* alleles. The KpnI restriction enzyme sites used for Southern blot analysis are marked with "K," and the new KpnI site introduced by the targeting vector is marked with "K*." The location of the 5′ probe used for Southern blot analysis is also indicated, as are the locations of the genotyping primers (green arrows). **B,** Southern blot analysis of KpnI-digested genomic DNA from *Pkm1*$^{+/+}$ (+/+), *Pkm1*$^{+/fl}$ (f/+), and *Pkm1*$^{fl/fl}$ (f/f) mice using the 5′ probe shown in **A**. Digestion of genomic DNA harboring the wild-type allele (+) yields an 8.3 kb fragment, whereas DNA harboring the floxed allele (f) yields a ∼5.0 kb fragment. **C,** *Pkm1* mRNA levels in anterior prostate tissue from wild-type (WT) and *Pkm1*$^{fl/fl}$ *PbCre4* (Pkm1$^{pc-/-}$) mice as determined by qRT-PCR. Mean ± SD is shown ($n = 5$). The difference in expression between genotypes is significant (***, $P < 0.001$ by Student *t* test). **D,** Western blot analysis of PKM1 and PKM2 expression in the indicated tissues from WT and Pkm1$^{pc-/-}$ mice. DLP, dorsolateral prostate; WAT, white adipose tissue.

expression is retained in other PKM1-expressing tissues (**Fig. 2D**). Loss of PKM1 in the prostate also resulted in increased PKM2 expression in all three prostate lobes relative to other tissues (**Fig. 2D**). These results confirm the conditional allele functions as designed, and demonstrates that deletion of *Pkm1* results in increased *Pkm2* expression in mouse prostate tissue.

Pkm1 deletion promotes prostate cancer progression

To determine the effect of *Pkm1* deletion on prostate tumor initiation and progression, we crossed $Pkm1^{fl/fl}$ mice to $Pten^{pc-/-}$ mice (hereafter, $Pkm1;Pten^{pc-/-}$). We found that the survival of $Pkm1;Pten^{pc-/-}$ animals was decreased compared with $Pten^{pc-/-}$ animals (**Fig. 3A**). Tumors were never observed in $Pkm1^{pc-/-}$ mice without

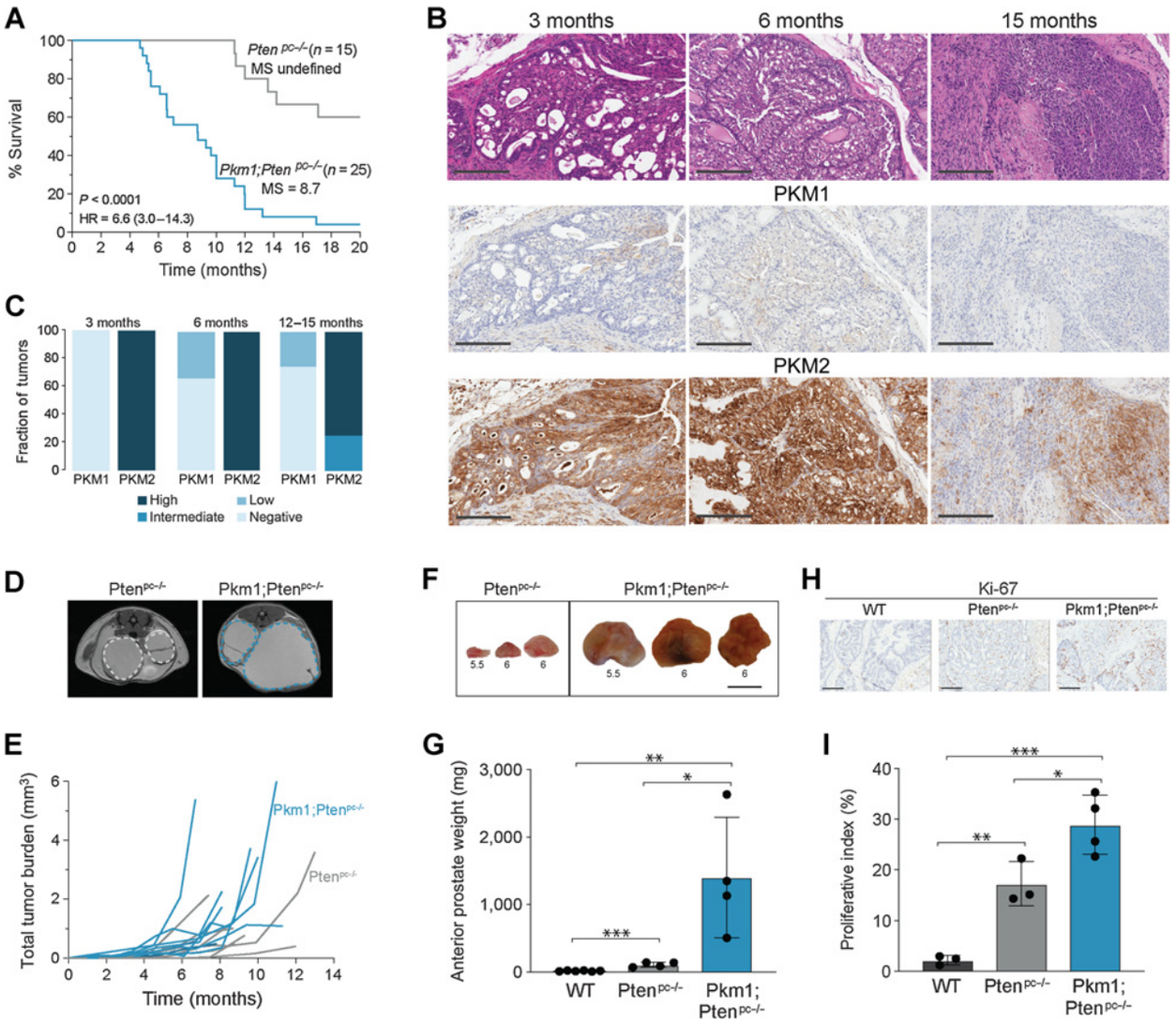

Figure 3.

Pkm1 deletion promotes progression of *Pten*-null prostate cancer. **A,** Kaplan–Meier curve assessing survival of a cohort of $Pten^{pc-/-}$ and $Pkm1;Pten^{pc-/-}$ mice as indicated. *P* value shown is for comparison of survival curves by log-rank test. Median survival (MS) and HR for death with 95% CI were determined by Mantel–Haenszel test with $Pten^{pc-/-}$ as comparator group. **B,** Representative hematoxylin and eosin and IHC assessment of PKM1 and PKM2 expression in prostate tissue harvested from $Pkm1;Pten^{pc-/-}$ mice of the indicated age. Scale bar, 200 μm. **C,** Quantitation of PKM1 and PKM2 expression in prostate tissue harvested from $Pkm1;Pten^{pc-/-}$ mice of the indicated age as determined by IHC. Tissue from 3 to 4 mice per age group was quantified. **D,** Representative MRI image of 6-month-old $Pten^{pc-/-}$ and $Pkm1;Pten^{pc-/-}$ mice. The left and right anterior prostates are outlined in each image. **E,** Prostate tumor volume estimated from serial MRI scans over time for a cohort of $Pten^{pc-/-}$ and $Pkm1;Pten^{pc-/-}$ mice as shown. Each line represents data from a single mouse, with the age of each mouse corresponding to time on the *x*-axis. **F,** Representative macroscopic images of anterior prostate tissue dissected from $Pten^{pc-/-}$ or $Pkm1;Pten^{pc-/-}$ mice as indicated. The age of the mouse in months at the time tissue was harvested is shown below each specimen. Scale bar, 1 cm. **G,** Weight of anterior prostate tissue dissected from 6-month-old WT, $Pten^{pc-/-}$ and $Pkm1;Pten^{pc-/-}$ mice. Mean ± SD is shown (WT, $n = 6$; $Pten^{pc-/-}$, $n = 4$; and $Pkm1;Pten^{pc-/-}$, $n = 4$). Differences in tissue weight are significant. **H,** Representative Ki-67 IHC of anterior prostate tissue harvested from 6-month-old WT, $Pten^{pc-/-}$ and $Pkm1;Pten^{pc-/-}$ mice. Scale bar, 200 μm. **I,** Proliferative index of anterior prostate tissue from 6-month-old WT, $Pten^{pc-/-}$, and $Pkm1;Pten^{pc-/-}$ mice as determined by Ki-67 IHC. Mean ±SD is shown (WT, $n = 4$; $Pten^{pc-/-}$, $n = 3$; and $Pkm1;Pten^{pc-/-}$, $n = 4$). Differences in proliferative index are significant. *, $P < 0.05$, **, $P < 0.01$; ***, $P < 0.001$ by Student *t* test.

Pten deletion when aged to 15 months, suggesting *Pkm1* loss may accelerate cancer initiated by *Pten* deletion. Indeed, prostate tumors in *Pkm1;Pten*$^{pc-/-}$ animals showed loss of *Pkm1* expression and strong *Pkm2* expression at earlier time points than in *Pten*$^{pc-/-}$ animals (**Figs. 1C** and **D** and **3B** and **C**), and histopathologic analysis showed *Pkm1;Pten*$^{pc-/-}$ animals developed invasive adenocarcinoma more frequently in younger mice than *Pten*$^{pc-/-}$ littermates (Supplementary Fig. S3A). *Pkm1;Pten*$^{pc-/-}$ tumors stained positive for pancytokeratin and negative for vimentin consistent with prostate epithelial origin (Supplementary Fig. S3B). Like tumors in *Pten*$^{pc-/-}$ mice (Supplementary Fig. S1D), they also stained positive for the androgen receptor (AR; Supplementary Fig. S3C). Focal synaptophysin expression was observed in a tumor harvested from a 15-month-old *Pkm1;Pten*$^{pc-/-}$ animal (Supplementary Fig. S3B), suggesting that at late stages these tumors may undergo neuroendocrine differentiation as has been observed in younger animals with prostate cancer driven by *Rb* loss or N-myc overexpression in combination with *Pten* loss (62, 63). However, this phenotype was not investigated further because most *Pkm1;Pten*$^{pc-/-}$ animals did not survive beyond 1 year (**Fig. 3A**).

Serial MRI showed that tumors in *Pkm1;Pten*$^{pc-/-}$ animals arose earlier and grew faster than tumors in *Pten*$^{pc-/-}$ animals (**Fig. 3D** and **E**). Analysis of prostate tissue from 6-month-old mice, a time where high-grade PIN and adenocarcinoma are observed in *Pten*$^{pc-/-}$ mice (Supplementary Fig. S3A; ref. 21), demonstrated that *Pkm1;Pten*$^{pc-/-}$ animals have larger tumors than *Pten*$^{pc-/-}$ mice, and prostate weight in *Pkm1;Pten*$^{pc-/-}$ mice is greater than that found in both *Pten*$^{pc-/-}$ and wild-type (WT) control mice (**Fig. 3F** and **G**). Ki-67 staining indicated increased proliferation in *Pkm1;Pten*$^{pc-/-}$ tumors relative to *Pten*$^{pc-/-}$ tumors and WT prostate tissue (**Fig. 3H** and **I**). We found no evidence of macroscopic metastases in animals of either genotype at either 6 or 12 months of age. These data argue *Pkm1* deletion accelerates growth of *Pten*-loss-driven prostate tumors.

Pkm2 deletion suppresses prostate cancer formation

To determine whether *Pkm2* is required for prostate tumor initiation and/or progression, we crossed *Pkm2*-conditional mice (*Pkm2*$^{fl/fl}$; ref. 45) to *Pten*$^{pc-/-}$ mice (hereafter, *Pkm2;Pten*$^{pc-/-}$). In contrast to both *Pten*$^{pc-/-}$ and *Pkm1;Pten*$^{pc-/-}$ mice, most *Pkm2;Pten*$^{pc-/-}$ mice lived a normal lifespan. We therefore assessed prostate size by serial MRI and found a striking delay in abnormal prostate growth in *Pkm2;Pten*$^{pc-/-}$ mice compared with *Pten*$^{pc-/-}$ littermates (**Fig. 4A**), although some ultimately developed PIN and/or invasive cancer (Supplementary Fig. S3A). Analysis of prostate tissue in *Pkm2;Pten*$^{pc-/-}$ mice younger than 12 months showed nearly normal appearing prostates in many animals even though all *Pten*$^{pc-/-}$ littermates developed PIN lesions or invasive cancer by 6 months of age (Supplementary Fig. S3A). We confirmed loss of PKM2 expression in prostate tissue from *Pkm2;Pten*$^{pc-/-}$ mice and observed strong expression of PKM1 (**Fig. 4B** and **C**). Deletion of *Pkm2* had no effect on AR expression and lesions arising in these mice stained positive for pancytokeratin and negative for vimentin and synaptophysin (Supplementary Fig. S4). Delayed prostate tumor progression observed by MRI (**Fig. 4A**, **D**, and **E**) was confirmed at time of necropsy, where we found that prostates from 14- to 15-month-old *Pkm2;Pten*$^{pc-/-}$ animals were smaller and weighed less than prostates from 6-month-old *Pten*$^{pc-/-}$ littermates (**Fig. 4F** and **G**). Furthermore, Ki-67 staining suggested decreased proliferation in 6-month-old *Pkm2;Pten*$^{pc-/-}$ prostates compared with *Pten*$^{pc-/-}$ animals (**Fig. 4H** and **I**). These data suggest PKM2 rather than PKM1 expression may be necessary for tumorigenesis in this tissue, and when considered together with results from *Pkm1;Pten*$^{pc-/-}$ mice, are consistent with PKM1 expression being tumor suppressive in the prostate.

Pkm2 deletion alters metabolism and promotes DNA replication stress and cellular senescence in *Pten* null prostate tissue

To assess whether pyruvate kinase isoform expression affects glucose uptake in the prostate, 6-month-old WT, *Pten*$^{pc-/-}$, *Pkm1;Pten*$^{pc-/-}$, and *Pkm2;Pten*$^{pc-/-}$ mice were imaged with FDG-PET. Consistent with PKM2 deletion leading to reduced neoplasia, prostates from *Pkm2;Pten*$^{pc-/-}$ mice exhibited glucose uptake that was similar to WT animal prostates, and lower than that observed in prostates from *Pten*$^{pc-/-}$ and *Pkm1;Pten*$^{pc-/-}$ mice (**Fig. 5A**). These data suggest that a shift from PKM2 to PKM1 expression in prostates of *Pkm2;Pten*$^{pc-/-}$ mice suppresses the increased glucose uptake associated with prostate neoplasia in *Pten*$^{pc-/-}$ and *Pkm1;Pten*$^{pc-/-}$ mice.

In mouse embryonic fibroblasts, PKM1-mediated suppression of cell proliferation is due to altered metabolism that results in nucleotide depletion and impaired DNA replication (31). To determine whether changes in metabolite levels are correlated with pyruvate kinase isoform expression and/or prostate tumor growth, we examined metabolite levels in the anterior prostates from 6-month-old WT, *Pten*$^{pc-/-}$, *Pkm1;Pten*$^{pc-/-}$, and *Pkm2;Pten*$^{pc-/-}$ mice (Supplementary Data File S1). Principle component analysis found that metabolite levels in WT prostate tissue are distinct from *Pten* null prostate tissue regardless of *Pkm* genotype, consistent with an effect of Pten loss on metabolism (**Fig. 5B**). Compared with *Pten*$^{pc-/-}$ and *Pkm1;Pten*$^{pc-/-}$ prostate tissue, which clustered together, *Pkm2;Pten*$^{pc-/-}$ prostate tissue clustered separately consistent with prostate neoplasia being suppressed in these mice (**Fig. 5B**). Interestingly, the majority of metabolites that were significantly different between *Pkm2;Pten*$^{pc-/-}$ and *Pten*$^{pc-/-}$ prostate tissue were related to nucleotide and redox metabolism (Supplementary Table S1; **Fig. 5C**). Specifically, when compared with *Pten*$^{pc-/-}$ prostate tissue, *Pkm2;Pten*$^{pc-/-}$ prostate tissue exhibited increased levels of several nucleosides and decreased levels of two nucleotide monophosphates as well as ribose-1-phosphate. Elevated nucleosides is suggestive of impaired salvage, which when coupled with decreased levels of nucleotide precursors may be indicative of impaired nucleotide metabolism in *Pkm1* expressing prostate tissue. Prostate tissue from *Pkm2;Pten*$^{pc-/-}$ mice also showed increased levels of 3-hydroxybutyrate (β-hydroxybutyrate) and lactate, potentially suggestive of a more reduced tissue redox state that would also be predicted to impair nucleotide synthesis (10, 64). Of note, none of these metabolites were significantly different when comparing tissue from *Pkm1;Pten*$^{pc-/-}$ and *Pten*$^{pc-/-}$ mice (Supplementary Table S1). Taken together, these data suggest that loss of PKM2 leading to PKM1 expression in the setting of Pten loss may affect nucleotide metabolism, possibly contributing to tumor suppression.

Impaired nucleotide synthesis can lead to DNA replication stress, which initiates a signaling response that leads to CHK1 phosphorylation and can be a barrier to tumor progression (65, 66). Consistent with published reports (26), we observed increased phospho-CHK1 staining indicative of DNA replication stress in prostate tissue from 6-month-old *Pten*-null mice (Supplementary Fig. S5A). Interestingly, prominent phospho-CHK1 staining persists in PKM1-expressing prostate tissue from *Pkm2;Pten*$^{pc-/-}$ mice and is lost as tumors progress in *Pkm1;Pten*$^{pc-/-}$ mice (**Fig. 5D** and **E**; Supplementary Fig. S5B). Nucleotide depletion can also underlie oncogene-induced senescence (25), and *Pten* deletion in the prostate initially results in cellular senescence that is overcome with time, or by *Trp53* deletion (21). To evaluate whether tumor suppression by *Pkm2* loss is associated with maintenance of senescence, we examined SA-β-gal staining as a

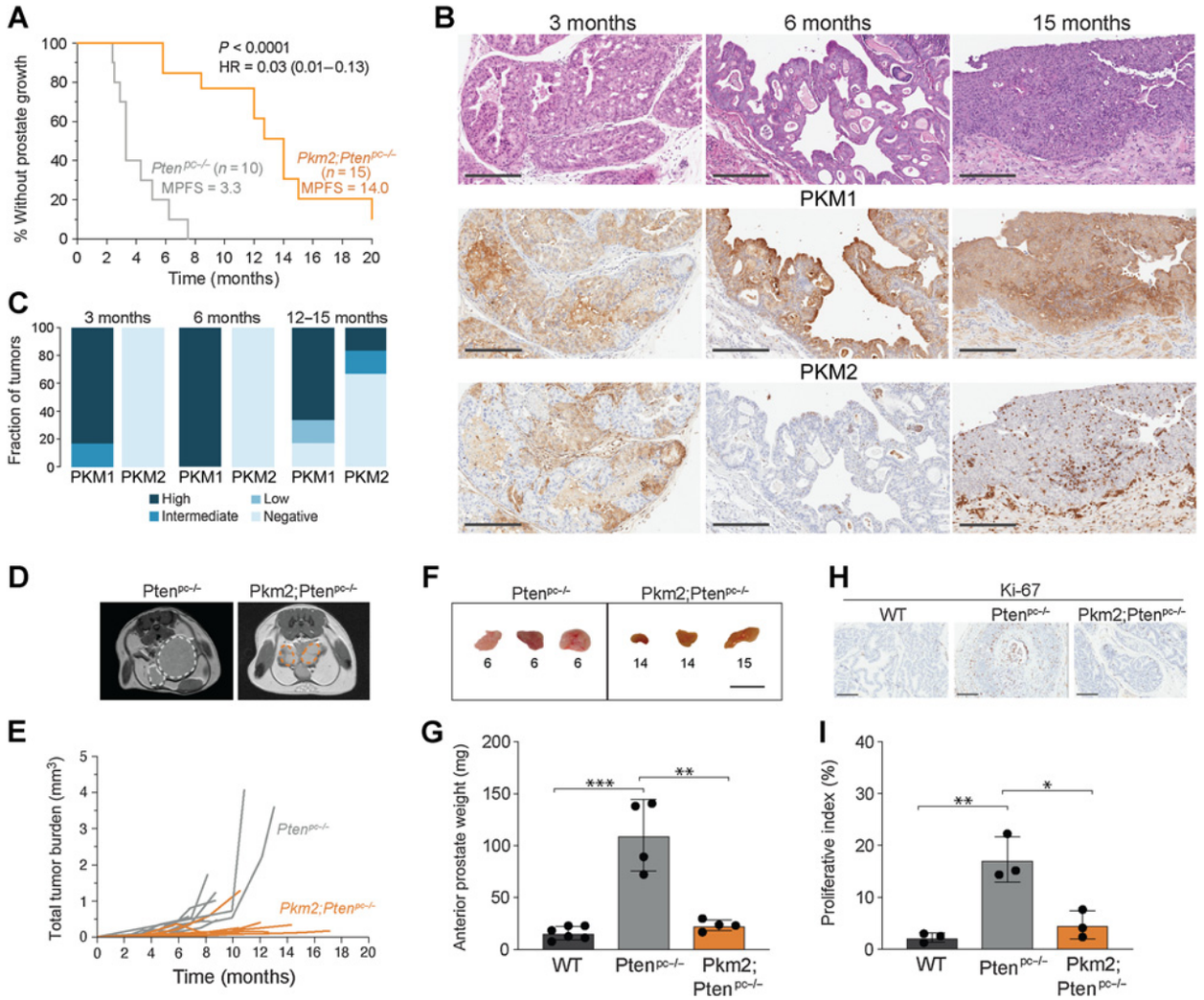

Figure 4.

Pkm2 deletion slows progression of *Pten*-null prostate cancer. **A,** Kaplan–Meier curve assessing the onset of abnormal prostate growth as determined by serial MRI in $Pten^{pc-/-}$ and $Pkm2;Pten^{pc-/-}$ mice. The difference in time to abnormal prostate growth is significant. Median progression-free survival (MPFS) and HR for radiographic progression with 95% CI were determined by Mantel–Haenszel test with $Pten^{pc-/-}$ as comparator group. **B,** Representative hematoxylin and eosin and IHC assessment of PKM1 and PKM2 expression in prostate tissue harvested from $Pkm2;Pten^{pc-/-}$ mice of the indicated age. Scale bar, 200 μm. **C,** Quantitation of PKM1 and PKM2 expression in prostate tissue harvested from $Pkm2;Pten^{pc-/-}$ mice of the indicated age as determined by IHC. Tissue from 3 to 6 mice per age group was quantified. **D,** Representative MRI image of 6-month-old $Pten^{pc-/-}$ and $Pkm2;Pten^{pc-/-}$ mice. The left and right anterior prostates are outlined in each image. **E,** Prostate tumor volume estimated from serial MRI scans over time for a cohort of $Pten^{pc-/-}$ and $Pkm2;Pten^{pc-/-}$ mice as shown. Each line represents data from a single mouse, with the age of each mouse corresponding to time on the *x*-axis. **F,** Representative macroscopic images of anterior prostate tissue dissected from $Pten^{pc-/-}$ or $Pkm2;Pten^{pc-/-}$ mice as indicated. The age of the mouse in months at the time tissue was harvested is shown below each specimen. Scale bar, 1 cm. **G,** Weight of anterior prostate tissue dissected from 6-month-old WT and $Pten^{pc-/-}$ mice, and 14- to 15-month-old $Pkm2;Pten^{pc-/-}$ mice. Mean ± SD is shown (WT, $n = 6$; $Pten^{pc-/-}$, $n = 4$; and $Pkm2;Pten^{pc-/-}$, $n = 4$). The indicated differences in tissue weight are significant. **H,** Representative Ki-67 IHC of anterior prostate tissue harvested from 6-month-old WT, $Pten^{pc-/-}$ and $Pkm2;Pten^{pc-/-}$ mice. Scale bar, 200 μm. **I,** Proliferative index of anterior prostate tissue harvested from 6-month-old WT, $Pten^{pc-/-}$, and $Pkm2;Pten^{pc-/-}$ mice as determined by Ki-67 IHC. Mean ± the SD is shown (WT, $n = 4$; $Pten^{pc-/-}$, $n = 3$; and $Pkm2;Pten^{pc-/-}$, $n = 3$). The indicated differences in proliferative index are significant. *, $P < 0.05$; **, $P < 0.01$; ***, $P < 0.001$ by Student *t* test.

marker of senescence in prostate tissue from 6-month-old WT, $Pten^{pc-/-}$, $Pkm1;Pten^{pc-/-}$, and $Pkm2;Pten^{pc-/-}$ animals. We observed increased SA-β-gal staining specifically in prostate epithelial cells in tissue from 6-month-old $Pten;Pkm2^{pc-/-}$ animals as compared with tissue from age-matched WT, $Pten^{pc-/-}$, and $Pkm1;Pten^{pc-/-}$ mice (**Fig. 5F**). Taken together these data suggest that PKM1 deletion leading to PKM2 expression allows tumors induced by *Pten* loss to overcome replication stress, whereas PKM2 deletion leading to PKM1 expression promotes persistent *Pten* loss-induced replication stress and senescence.

Pharmacologic activation of PKM2 in $Pten^{pc-/-}$ mice delays prostate tumor growth

Because *Pkm1* encodes a constitutively active enzyme, and low pyruvate kinase activity can promote tumor growth (40, 45), we hypothesized that activating PKM2, thereby forcing it into a

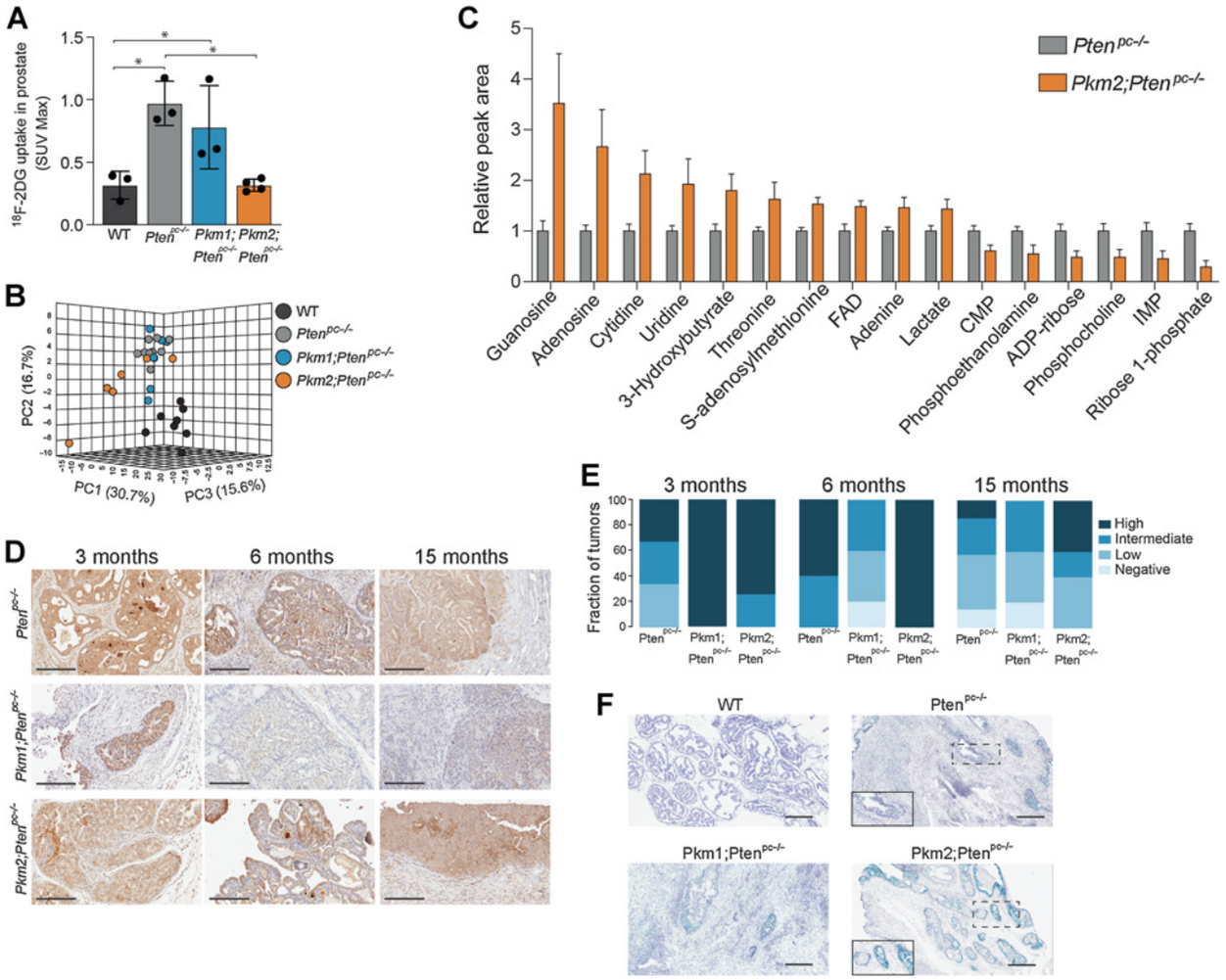

Figure 5.

Pkm2 deletion suppresses increased glucose uptake, affects metabolite levels, and prolongs DNA replication stress and cellular senescence in *Pten*-null prostate tissue. **A,** Maximum relative [^{18}F]fluoro-2-deoxyglucose signal (SUV Max) in prostate tissue as assessed by PET of 6-month-old WT, $Pten^{pc-/-}$, *Pkm1*;$Pten^{pc-/-}$, and *Pkm2*;$Pten^{pc-/-}$ mice. Prostate signal normalized to the intensity of the emission spectra in the heart of the same mouse is shown (WT, $n = 3$; $Pten^{pc-/-}$, $n = 3$; *Pkm1*;$Pten^{pc-/-}$, $n = 3$; *Pkm2*;$Pten^{pc-/-}$, $n = 4$). The indicated differences in FDG uptake are significant. *, $P < 0.05$ by Student *t* test. **B,** Principle component analysis of 111 polar metabolites measured by LC/MS in prostate tissue harvested from 6-month-old WT, $Pten^{pc-/-}$, *Pkm1*;$Pten^{pc-/-}$, and *Pkm2*;$Pten^{pc-/-}$ mice (WT, $n = 8$; $Pten^{pc-/-}$, $n = 10$; *Pkm1*;$Pten^{pc-/-}$, $n = 6$; *Pkm2*;$Pten^{pc-/-}$, $n = 6$). **C,** Relative levels of all metabolites measured by LC/MS that were significantly different ($P < 0.05$ by Student *t* test) in a comparison of prostate tissue harvested from 6-month-old $Pten^{-/-}$ or *Pkm2*;$Pten^{-/-}$ mice ($Pten^{pc-/-}$, $n = 10$; *Pkm2*;$Pten^{pc-/-}$, $n = 6$). **D,** Representative IHC staining for phospho-CHK1 in prostate tissue harvested from $Pten^{pc-/-}$, *Pkm1*;$Pten^{pc-/-}$, and *Pkm2*;$Pten^{pc-/-}$ mice of the indicated age. Scale bar, 200 μm. **E,** Quantitation of phospho-CHK1 staining in prostate tissue harvested from $Pten^{pc-/-}$, *Pkm1*;$Pten^{pc-/-}$, and *Pkm2*;$Pten^{pc-/-}$ mice of the indicated age as determined by IHC. Tissue from 3 to 6 mice per age group was quantified. **F,** Representative SA-β-gal staining of anterior prostate tissue harvested from 6-month-old WT, $Pten^{pc-/-}$, *Pkm1*;$Pten^{pc-/-}$, and *Pkm2*;$Pten^{pc-/-}$ mice. The area indicated by the dashed box is shown larger in the lower left inset for the right two panels. Scale bar, 500 μm.

high-activity PKM1-like state might suppress tumor growth in $Pten^{pc-/-}$ mice. To test this, we randomized $Pten^{pc-/-}$ mice with established tumors to treatment with vehicle or TEPP-46, an orally bioavailable PKM2 activator (30), that was administered twice a day for 1 month. Tumor size was assessed at baseline and biweekly over the course of therapy using MRI. Most tumors from vehicle-treated $Pten^{pc-/-}$ mice increased in size (as defined by >50% change in tumor volume) over the 1-month period of treatment, whereas fewer tumors from TEPP-46 treated animals grew over the same time period, with radiographic evidence of tumor shrinkage in some mice (**Fig. 6A** and **B**; Supplementary Fig. S6A). The proliferation index as assessed by Ki-67 staining also decreased in tumors treated for 1 month with TEPP-46 (**Fig. 6C**; Supplementary Fig. S6B). These data suggest that pharmacologic activation of PKM2 can suppress prostate tumor growth and supports the notion that high pyruvate kinase activity is tumor suppressive in this tissue.

Human prostate cancers exhibit moderate to high levels of Pkm2 expression

Pkm2 expression is variable in many human cancers (33, 45, 48, 50) and knowing whether this is also the case in human prostate cancer is important to consider PKM2 activators as potential therapeutics.

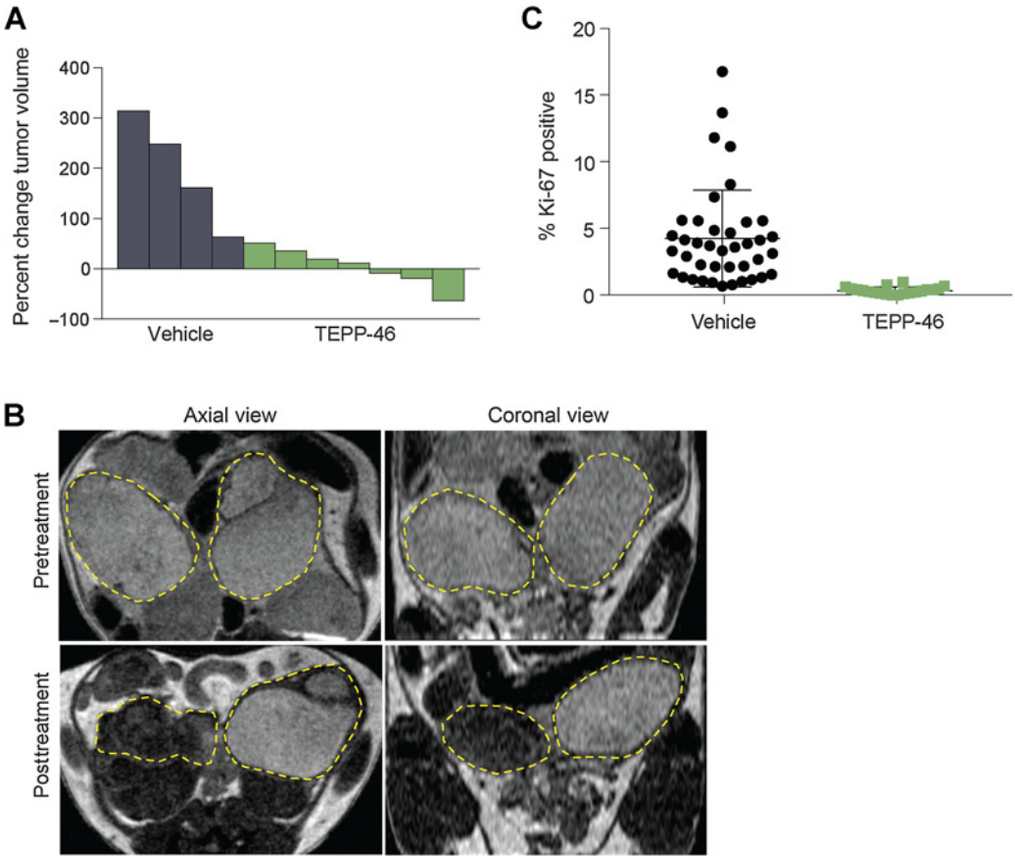

Figure 6.

PKM2 activator treatment reduces *Pten*$^{pc-/-}$ mouse prostate tumor growth. **A,** Waterfall plot showing the maximal change in total mouse prostate tumor volume as assessed by MRI in tumor-bearing *Pten*$^{pc-/-}$ mice after 1 month of twice a day treatment with vehicle or 50 mg/kg of TEPP-46 as indicated (vehicle, $n = 4$; TEPP-46, $n = 7$). **B,** Representative MRI images from a tumor-bearing *Pten*$^{pc-/-}$ mouse dosed with TEPP-46 twice a day for 1 month. Axial and coronal view images from the same approximate anatomical plane are shown pre- and post-treatment as indicated. The left and right anterior prostates are outlined in each image. **C,** Proliferative index as determined by Ki-67 IHC of prostate tumors from *Pten*$^{pc-/-}$ mice treated with vehicle or TEPP-46 as indicated.

Thus, PKM2 expression was examined using IHC in sections from patients who underwent prostatectomy and in prostate cancer specimens on a prostate tumor microarray (TMA; **Fig. 7**). PKM2 expression was noted in some epithelial cells in normal prostate tissue, and was retained in cancer cells in both low- and high-grade tumors, whereas PKM1 expression was restricted to the stromal regions of both normal and malignant prostate tissue. Of note, we observed that most human prostate tumors exhibit some PKM2 expression, with intermediate to high PKM2 expression found in more than half of tumors including higher Gleason grade cancers and tumors from patients with more advanced disease (**Fig. 7B** and **C**). These data suggest that unlike some other human cancers, PKM2 expression is retained even in clinically aggressive prostate cancer, arguing that PKM2 activation may be effective in treating patients with this disease.

Discussion

Modulation of pyruvate kinase isoform expression has large effects on *Pten* loss-driven prostate tumor initiation and growth. Despite the fact that PKM2 is the predominant isoform expressed in most human and mouse cancers, *Pkm2* expression is dispensable for the formation and growth of multiple other cancer types. Deletion of *Pkm2* in autochthonous models of breast cancer, acute myeloid leukemia, colon cancer, medulloblastoma, pancreatic cancer, hepatocellular carcinoma, and sarcoma has minimal effect on cancer growth, and in some cases accelerates cancer progression (33, 45–50). Thus, a tumor suppressive effect of *Pkm2* deletion in prostate tissue appears to be the exception among mouse cancer models examined to date.

In many mouse cancer models where *Pkm2* loss does not affect tumor growth, loss of *Pkm2* is accompanied by minimal to undetectable PKM1 expression (33, 45–50). In prostate tissue, high PKM1 expression accompanies *Pkm2* deletion. The relative correlation between PKM1 expression and tumor suppression in various autochthonous cancer models is consistent with a tumor suppressive role for high pyruvate kinase activity. Ectopic PKM1 expression has been shown to suppress both mouse and human tumor growth in mice, even in settings where PKM2 is not deleted and there is no selective pressure to retain PKM2 (29, 30, 45). Nevertheless, some tumors can grow despite retaining some PKM1 expression (46, 49) and a protumorigenic role for PKM1 has been reported in pulmonary neuroendocrine cancers (38). However, our finding that *Pkm1* deletion in *Pten* null prostate tissue results in aggressive cancers is strongly supportive of a tumor suppressive role for PKM1 in this organ.

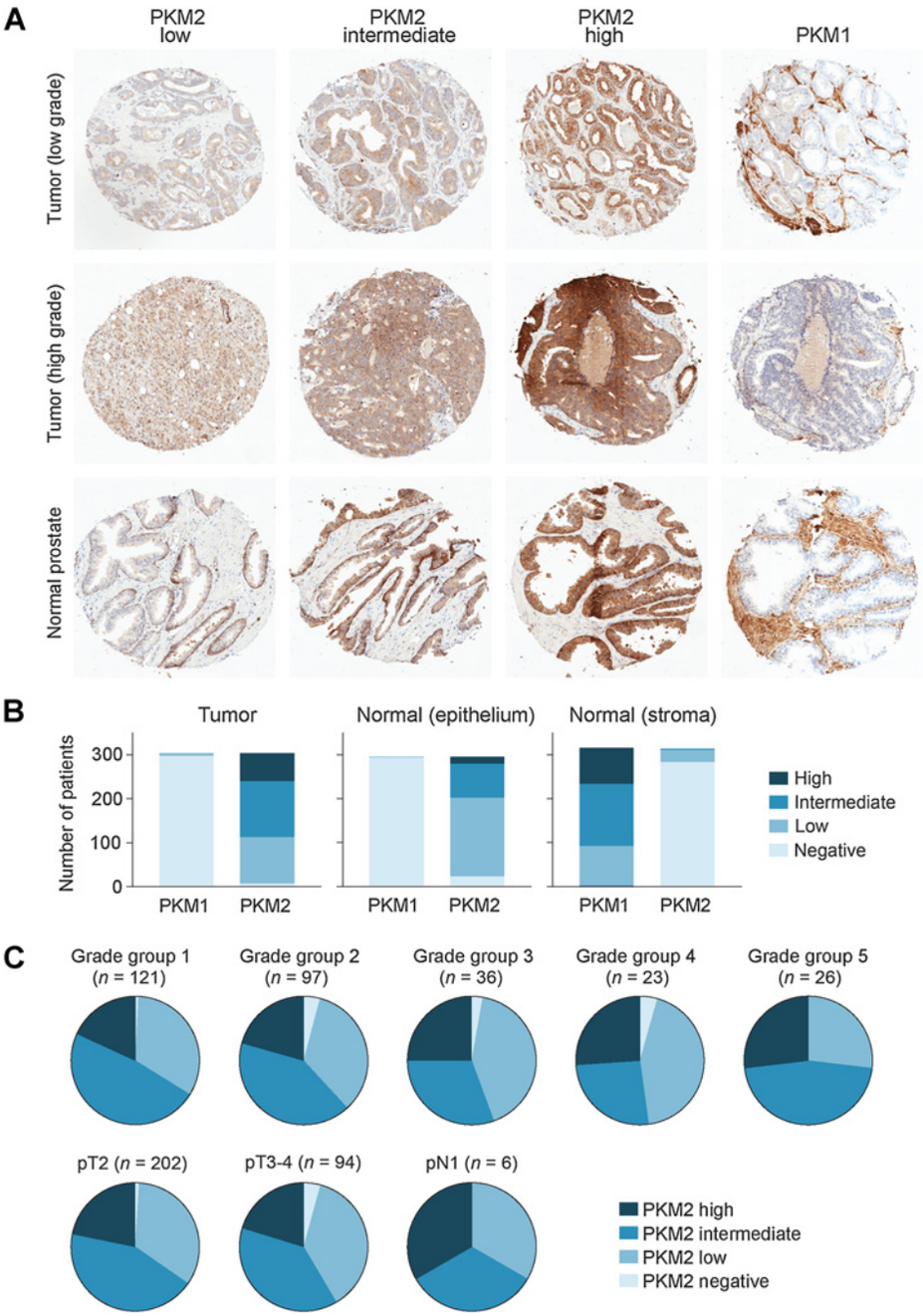

Figure 7.
PKM1 and PKM2 expression in normal and cancerous human prostate tissue. **A,** Representative IHC staining of PKM2 and PKM1 expression in low- and high-grade human prostate tumors and normal human prostate tissue is shown. Staining scored as low, intermediate, and high expression for PKM2 is indicated. The diameter of each tissue core is approximately 0.6 mm. **B,** Quantification of PKM1 and PKM2 expression by IHC in human prostate tissue (tumor and normal) present on a tissue array containing 304 samples. Expression level is based on the scoring rubric shown in **A**. **C,** Quantification of PKM2 expression by IHC in a human prostate cancer tissue array stratified by Gleason grade and TNM stage at the time of radical prostatectomy. The number of cases analyzed for each subset is indicated.

The mechanism by which PKM1 suppresses prostate tumor growth is not fully understood, although the fact that treating mice with PKM2 activators can phenocopy PKM1 expression suggests that high pyruvate kinase activity associated with PKM1 is involved. One mechanism by which high pyruvate kinase activity can suppress proliferation is by affecting nucleotide synthesis (31). Nucleotide depletion can promote cellular senescence (25), and an ability to overcome senescence is a barrier to prostate cancer initiation following *Pten* loss (21). Nucleotide depletion can also lead to DNA replication stress (25), and DNA replication stress downstream of *Pten* loss can lead to senescence of prostate epithelial cells (26). The observation that shifting from PKM1 to PKM2 expression during prostate cancer development impacts nucleotide metabolism and DNA replication stress signaling suggests that a change in pyruvate kinase isoform expression to enable less enzyme activity may support nucleotide synthesis and help cancer cells to overcome *Pten* loss-induced DNA replication stress and senescence.

Why high pyruvate kinase activity is particularly tumor suppressive in prostate tissue is not clear; however, it could be related to the distinct metabolic phenotype of this organ. Prostate tissue synthesizes both citrate and fructose for seminal fluid (67), and either PKM1 expression or PKM2 activation can promote oxidative glucose metabolism that may promote citrate synthesis (29, 30). A role for high pyruvate kinase

to support normal prostate tissue metabolism may explain in part why PKM1 is expressed in some normal prostate epithelial cells, as well as explain why loss of both PKM1 and PKM2 expression is less prevalent in prostate cancer as compared with other malignancies.

The finding that PKM2 is dispensable for tumor growth in multiple model systems, and that some cancer cells appear to proliferate despite undetectable expression of either PKM1 or PKM2 (33, 44–50), suggests that the effectiveness of small molecule pyruvate kinase activators in treating cancer will be limited by loss of pyruvate kinase expression, even though molecules that activate pyruvate kinase appear to be well tolerated in both mice and humans (30, 68, 69). However, the finding that PKM2 is retained in the majority of human prostate cancers and that either genetic or pharmacological manipulation of pyruvate kinase appears to be tumor suppressive in an autochthonous mouse model suggests that prostate cancer might be an indication where pyruvate kinase activation could be effective for therapy. Further work is needed to test this hypothesis in additional prostate cancer models, as well as uncover how pyruvate kinase activation interacts with existing prostate cancer therapies, and inform how these agents should be tested in patients with prostate cancer.

Authors' Disclosures

W.J. Israelsen reports grants from NIH during the conduct of the study. E. Freinkman reports personal fees from Immunai outside the submitted work and also has a patent 20200033360 pending. K.D. Courtney reports grants from Astellas and personal fees from Exelixis outside the submitted work. A. Jha reports other support from Elucidata Corporations outside the submitted work. R.A. DePinho reports grants from NIH during the conduct of the study, personal fees and other support from Tvardi Therapeutics, Asylia Therapeutics, Stellanova Therapeutic, and Nirogy Therapeutics, and other support from Sporos Bioventures outside the submitted work. C.J. Thomas reports a patent that cover the lead PKM2 activators used in this study issued. L.C. Cantley reports grants from NCI R35 CA197588 during the conduct of the study; personal fees and other support from Novartis, Volastra, Larkspur, and Faeth,; grants, personal fees, and other support from Petra; and grants from Stand up for Cancer/AACR outside the submitted work; also has a patent for WO 2008019139A3 and WO 2009025781A1 pending, licensed, and with royalties paid from Agios. M.G. Vander Heiden reports personal fees from Agios Pharmaceuticals, iTeos Therapeutics, Droia Ventures, Sage Therapeutics, Faeth Therapeutics, and Auron Therapeutics outside the submitted work and also has a patent for Use of pyruvate kinase activators to treat cancer issued and licensed to Agios Pharmaceutics. No disclosures were reported by the other authors.

Authors' Contributions

S.M. Davidson: Conceptualization, formal analysis, funding acquisition, investigation, methodology, writing–original draft, writing–review and editing. **D.R. Schmidt:** Formal analysis, investigation, methodology, writing–review and editing. **J.E. Heyman:** Methodology, writing–review and editing. **J.P. O'Brien:** Methodology, writing–review and editing. **A.C. Liu:** Methodology, writing–review and editing. **W.J. Israelsen:** Methodology. **T.L. Dayton:** Methodology. **R. Sehgal:** Methodology. **R.T. Bronson:** Formal analysis. **E. Freinkman:** Methodology. **H.H. Mak:** Methodology. **G.N. Fanelli:** Formal analysis. **S. Malstrom:** Methodology. **G. Bellinger:** Methodology. **A. Carracedo:** Methodology. **P. Pandolfi:** Methodology. **K.D. Courtney:** Methodology. **A. Jha:** Methodology. **R.A. DePinho:** Funding acquisition. **J.W. Horner:** Methodology. **C.J. Thomas:** Methodology. **L.C. Cantley:** Resources, funding acquisition. **M. Loda:** Methodology. **M.G. Vander Heiden:** Conceptualization, resources, supervision, funding acquisition, investigation, methodology, writing–original draft, writing–review and editing.

Acknowledgments

The authors thank the Swanson Biotechnology Center for tissue processing and members of the Vander Heiden Laboratory for thoughtful discussions. They also thank John Frangioni for assistance with FDG-PET studies and B. Bevis for help generating figures. S.M. Davidson was supported by an NSF Graduate Research Fellowship and T32GM007287. E. Freinkman acknowledges support from W81XWH-15-1-0337 from the Department of Defense. D.R. Schmidt acknowledges support by the Joint Center for Radiation Therapy Foundation and the Harvard University KL2/Catalyst Medical Research Investigator Training award (TR002542). C.J. Thomas acknowledges support from the Division of Preclinical Innovation, National Center for Advancing Translational Research and the Center for Cancer Research, NCI. L.C. Cantley acknowledges support from R35CA197588. M.G. Vander Heiden acknowledges support from the Ludwig Center at MIT, the Burroughs Wellcome Fund, the Damon Runyon Cancer Research Foundation, the MIT Center for Precision Cancer Medicine, a Stand Up To Cancer Innovative Research Grant (Grant Number SU2C-AACR-IRG-09-16), the Emerald Foundation, the NIH (P30CA1405141, R35CA242379, R01CA168653, K08CA136983, P50CA090381), and a faculty scholar award from the Howard Hughes Medical Institute. Stand Up To Cancer is a division of the Entertainment Industry Foundation. The indicated SU2C grant is administered by the American Association for Cancer Research, the scientific partner of SU2C.

The costs of publication of this article were defrayed in part by the payment of page charges. This article must therefore be hereby marked *advertisement* in accordance with 18 U.S.C. Section 1734 solely to indicate this fact.

Received July 19, 2021; revised April 19, 2022; accepted May 11, 2022; published first May 18, 2022.

References

1. Siegel RL, Miller KD, Jemal A. Cancer statistics, 2020. CA Cancer J Clin 2020;70:7–30.
2. Gray IC, Stewart LM, Phillips SM, Hamilton JA, Gray NE, Watson GJ, et al. Mutation and expression analysis of the putative prostate tumour-suppressor gene PTEN. Br J Cancer 1998;78:1296–300.
3. Whang YE, Wu X, Suzuki H, Reiter RE, Tran C, Vessella RL, et al. Inactivation of the tumor suppressor PTEN/MMAC1 in advanced human prostate cancer through loss of expression. Proc Natl Acad Sci U S A 1998;95:5246–50.
4. Morgan TM, Koreckij TD, Corey E. Targeted therapy for advanced prostate cancer: inhibition of the PI3K/Akt/mTOR pathway. Curr Cancer Drug Targets 2009;9:237–49.
5. Testa JR, Tsichlis PN. AKT signaling in normal and malignant cells. Oncogene 2005;24:7391–3.
6. Song MS, Salmena L, Pandolfi PP. The functions and regulation of the PTEN tumour suppressor. Nat Rev Mol Cell Biol 2012;13:283–96.
7. Vivanco I, Sawyers CL. The phosphatidylinositol 3-Kinase AKT pathway in human cancer. Nat Rev Cancer 2002;2:489–501.
8. Pavlova NN, Thompson CB. The emerging hallmarks of cancer metabolism. Cell Metab 2016;23:27–47.
9. DeBerardinis RJ, Chandel NS. Fundamentals of cancer metabolism. Sci Adv 2016;2:e1600200.
10. Vander Heiden MG, DeBerardinis RJ. Understanding the intersections between metabolism and cancer biology. Cell 2017;168:657–69.
11. DeBerardinis RJ, Chandel NS. We need to talk about the Warburg effect. Nature Metabolism 2020;2:127–9.
12. Plathow C, Weber WA. Tumor cell metabolism imaging. J Nucl Med 2008;49:43S–63S.
13. Zadra G, Photopoulos C, Loda M. The fat side of prostate cancer. Biochim Biophys Acta 2013;1831:1518–32.
14. Effert P, Beniers AJ, Tamimi Y, Handt S, Jakse G. Expression of glucose transporter 1 (Glut-1) in cell lines and clinical specimens from human prostate adenocarcinoma. Anticancer Res 2004;24:3057–63.
15. Fendt SM, Bell EL, Keibler MA, Davidson SM, Wirth GJ, Fiske B, et al. Metformin decreases glucose oxidation and increases the dependency of prostate cancer cells on reductive glutamine metabolism. Cancer Res 2013;73:4429–38.
16. Beauregard JM, Blouin AC, Fradet V, Caron A, Fradet Y, Lemay C, et al. FDG-PET/CT for pre-operative staging and prognostic stratification of patients with high-grade prostate cancer at biopsy. Cancer Imaging 2015;15:2.

17. Jadvar H. Is there use for FDG-PET in prostate cancer? Semin Nucl Med 2016;46:502–6.
18. Perez-Mancera PA, Young AR, Narita M. Inside and out: the activities of senescence in cancer. Nat Rev Cancer 2014;14:547–58.
19. Kuilman T, Michaloglou C, Mooi WJ, Peeper DS. The essence of senescence. Genes Dev 2010;24:2463–79.
20. Collado M, Serrano M. Senescence in tumours: evidence from mice and humans. Nat Rev Cancer 2010;10:51–7.
21. Chen Z, Trotman LC, Shaffer D, Lin HK, Dotan ZA, Niki M, et al. Crucial role of p53-dependent cellular senescence in suppression of Pten-deficient tumorigenesis. Nature 2005;436:725–30.
22. Kaplon J, Zheng L, Meissl K, Chaneton B, Selivanov VA, Mackay G, et al. A key role for mitochondrial gatekeeper pyruvate dehydrogenase in oncogene-induced senescence. Nature 2013;498:109–12.
23. Dorr JR, Yu Y, Milanovic M, Beuster G, Zasada C, Dabritz JH, et al. Synthetic lethal metabolic targeting of cellular senescence in cancer therapy. Nature 2013;501:421–5.
24. Jiang P, Du W, Mancuso A, Wellen KE, Yang X. Reciprocal regulation of p53 and malic enzymes modulates metabolism and senescence. Nature 2013;493:689–93.
25. Aird KM, Zhang G, Li H, Tu Z, Bitler BG, Garipov A, et al. Suppression of nucleotide metabolism underlies the establishment and maintenance of oncogene-induced senescence. Cell Rep 2013;3:1252–65.
26. Parisotto M, Grelet E, El Bizri R, Dai Y, Terzic J, Eckert D, et al. PTEN deletion in luminal cells of mature prostate induces replication stress and senescence in vivo. J Exp Med 2018;215:1749–63.
27. Ashrafian H. Cancer's sweet tooth: the Janus effect of glucose metabolism in tumorigenesis. Lancet 2006;367:618–21.
28. Favaro E, Bensaad K, Chong MG, Tennant DA, Ferguson DJ, Snell C, et al. Glucose utilization via glycogen phosphorylase sustains proliferation and prevents premature senescence in cancer cells. Cell Metab 2012;16:751–64.
29. Christofk HR, Vander Heiden MG, Harris MH, Ramanathan A, Gerszten RE, Wei R, et al. The M2 splice isoform of pyruvate kinase is important for cancer metabolism and tumour growth. Nature 2008;452:230–3.
30. Anastasiou D, Yu Y, Israelsen WJ, Jiang JK, Boxer MB, Hong BS, et al. Pyruvate kinase M2 activators promote tetramer formation and suppress tumorigenesis. Nat Chem Biol 2012;8:839–47.
31. Lunt SY, Muralidhar V, Hosios AM, Israelsen WJ, Gui DY, Newhouse L, et al. Pyruvate kinase isoform expression alters nucleotide synthesis to impact cell proliferation. Mol Cell 2015;57:95–107.
32. Dayton TL, Jacks T., Vander Heiden MG. PKM2, cancer metabolism, and the road ahead. EMBO Rep 2016;17:1721–30.
33. Dayton TL, Gocheva V, Miller KM, Israelsen WJ, Bhutkar A, Clish CB, et al. Germline loss of PKM2 promotes metabolic distress and hepatocellular carcinoma. Genes Dev 2016;30:1020–33.
34. Chen M, David CJ, Manley JL. Concentration-dependent control of pyruvate kinase M mutually exclusive splicing by hnRNP proteins. Nat Struct Mol Biol 2012;19:346–54.
35. Gui DY, Lewis CA, Vander Heiden MG. Allosteric regulation of PKM2 allows cellular adaptation to different physiological states. Sci Signal 2013;6:pe7.
36. Mazurek S. Pyruvate kinase type M2: a key regulator of the metabolic budget system in tumor cells. Int J Biochem Cell Biol 2011;43:969–80.
37. Chaneton B, Gottlieb E. Rocking cell metabolism: revised functions of the key glycolytic regulator PKM2 in cancer. Trends Biochem Sci 2012;37:309–16.
38. Morita M, Sato T, Nomura M, Sakamoto Y, Inoue Y, Tanaka R, et al. PKM1 confers metabolic advantages and promotes cell-autonomous tumor cell growth. Cancer Cell 2018;33:355–67.
39. Israelsen WJ, Vander Heiden MG. Pyruvate kinase: Function, regulation and role in cancer. Semin Cell Dev Biol 2015;43:43–51.
40. Liu VM, Howell AJ, Hosios AM, Li Z, Israelsen WJ, Vander Heiden MG. Cancer-associated mutations in human pyruvate kinase M2 impair enzyme activity. FEBS Lett 2020;594:646–64.
41. Walsh MJ, Brimacombe KR, Veith H, Bougie JM, Daniel T, Leister W, et al. 2-Oxo-N-aryl-1,2,3,4-tetrahydroquinoline-6-sulfonamides as activators of the tumor cell specific M2 isoform of pyruvate kinase. Bioorg Med Chem Lett 2011;21:6322–7.
42. Yacovan A, Ozeri R, Kehat T, Mirilashvili S, Sherman D, Aizikovich A, et al. 1-(sulfonyl)-5-(arylsulfonyl)indoline as activators of the tumor cell specific M2 isoform of pyruvate kinase. Bioorg Med Chem Lett 2012;22:6460–8.
43. Parnell KM, Foulks JM, Nix RN, Clifford A, Bullough J, Luo B, et al. Pharmacologic activation of PKM2 slows lung tumor xenograft growth. Mol Cancer Ther 2013;12:1453–60.
44. Cortes-Cros M, Hemmerlin C, Ferretti S, Zhang J, Gounarides JS, Yin H, et al. M2 isoform of pyruvate kinase is dispensable for tumor maintenance and growth. Proc Natl Acad Sci U S A 2013;110:489–94.
45. Israelsen WJ, Dayton TL, Davidson SM, Fiske BP, Hosios AM, Bellinger G, et al. PKM2 isoform-specific deletion reveals a differential requirement for pyruvate kinase in tumor cells. Cell 2013;155:397–409.
46. Wang YH, Israelsen WJ, Lee D, Yu VW, Jeanson NT, Clish CB, et al. Cell-state-specific metabolic dependency in hematopoiesis and leukemogenesis. Cell 2014;158:1309–23.
47. Dayton TL, Gocheva V, Miller KM, Bhutkar A, Lewis CA, Bronson RT, et al. Isoform-specific deletion of PKM2 constrains tumor initiation in a mouse model of soft tissue sarcoma. Cancer Metab 2018;6:6.
48. Lau AN, Israelsen WJ, Roper J, Sinnamon MJ, Georgeon L, Dayton TL, et al. PKM2 is not required for colon cancer initiated by APC loss. Cancer Metab 2017;5:10.
49. Tech K, Tikunov AP, Farooq H, Morrissy AS, Meidinger J, Fish T, et al. Pyruvate kinase inhibits proliferation during postnatal cerebellar neurogenesis and suppresses medulloblastoma formation. Cancer Res 2017;77:3217–30.
50. Hillis AL, Lau AN, Devoe CX, Dayton TL, Danai LV, Di Vizio D, et al. PKM2 is not required for pancreatic ductal adenocarcinoma. Cancer Metab 2018;6:17.
51. Wang S, Gao J, Lei Q, Rozengurt N, Pritchard C, Jiao J, et al. Prostate-specific deletion of the murine Pten tumor suppressor gene leads to metastatic prostate cancer. Cancer Cell 2003;4:209–21.
52. Birbach A. Use of PB-Cre4 mice for mosaic gene deletion. PLoS One 2013;8:e53501.
53. Trotman LC, Niki M, Dotan ZA, Koutcher JA, Di Cristofano A, Xiao A, et al. Pten dose dictates cancer progression in the prostate. PLoS Biol 2003;1:E59.
54. Bankhead P, Loughrey MB, Fernandez JA, Dombrowski Y, McArt DG, Dunne PD, et al. QuPath: Open source software for digital pathology image analysis. Sci Rep 2017;7:16878.
55. Dimri GP, Lee X, Basile G, Acosta M, Scott G, Roskelley C, et al. A biomarker that identifies senescent human cells in culture and in aging skin in vivo. Proc Natl Acad Sci U S A 1995;92:9363–7.
56. Davidson SM, Papagiannakopoulos T, Olenchock BA, Heyman JE, Keibler MA, Luengo A, et al. Environment impacts the metabolic dependencies of ras-driven non-small cell lung cancer. Cell Metab 2016;23:517–28.
57. Dibble CC, Cantley LC. Regulation of mTORC1 by PI3K signaling. Trends Cell Biol 2015;25:545–55.
58. Wang L, Xiong H, Wu F, Zhang Y, Wang J, Zhao L, et al. Hexokinase 2-mediated Warburg effect is required for PTEN- and p53-deficiency-driven prostate cancer growth. Cell Rep 2014;8:1461–74.
59. Wu X, Wu J, Huang J, Powell WC, Zhang J, Matusik RJ, et al. Generation of a prostate epithelial cell-specific Cre transgenic mouse model for tissue-specific gene ablation. Mech Dev 2001;101:61–9.
60. Valkenburg KC, Williams BO. Mouse models of prostate cancer. Prostate Cancer 2011;2011:895238.
61. Zhang J, Thomas TZ, Kasper S, Matusik RJ. A small composite probasin promoter confers high levels of prostate-specific gene expression through regulation by androgens and glucocorticoids in vitro and in vivo. Endocrinology 2000;141:4698–710.
62. Ku SY, Rosario S, Wang Y, Mu P, Seshadri M, Goodrich ZW, et al. Rb1 and Trp53 cooperate to suppress prostate cancer lineage plasticity, metastasis, and antiandrogen resistance. Science 2017;355:78–83.
63. Dardenne E, Beltran H, Benelli M, Gayvert K, Berger A, Puca L, et al. N-Myc induces an EZH2-mediated transcriptional program driving neuroendocrine prostate cancer. Cancer Cell 2016;30:563–77.
64. Hosios AM, Vander Heiden MG. The redox requirements of proliferating mammalian cells. J Biol Chem 2018;293:7490–8.
65. Zeman MK, Cimprich KA. Causes and consequences of replication stress. Nat Cell Biol 2014;16:2–9.
66. Goto H, Kasahara K, Inagaki M. Novel insights into Chk1 regulation by phosphorylation. Cell Struct Funct 2015;40:43–50.
67. Costello LC, Franklin RB. The intermediary metabolism of the prostate: a key to understanding the pathogenesis and progression of prostate malignancy. Oncology 2000;59:269–82.
68. Qi W, Keenan HA, Li Q, Ishikado A, Kannt A, Sadowski T, et al. Pyruvate kinase M2 activation may protect against the progression of diabetic glomerular pathology and mitochondrial dysfunction. Nat Med 2017;23:753–62.
69. Grace RF, Rose C, Layton DM, Galacteros F, Barcellini W, Morton DH, et al. Safety and efficacy of mitapivat in pyruvate kinase deficiency. N Engl J Med 2019;381:933–44.